applied sciences

MDPI

Article

Silica-Based Sol-Gel Coating with High Transmission at 1053 and 527 nm and Absorption at 351 nm for Frequency-Converting Crystals in High-Power Laser System

Xue-Ran Deng [1], Wei Yang [1], Hao-Hao Hui [1], Qing-Hua Zhang [1], Qiao Xu [1], Jin-Ju Chen [2], Ji-Liang Zhu [3] and Xiang-Yang Lei [1,*]

1 Research Center of Laser Fusion, China Academy of Engineering Physics, No. 64 Mianshan Road, Mianyang 621900, China; xrdeng@foxmail.com (X.-R.D.); hch890@163.com (W.Y.); dream2001hui@163.com (H.-H.H.); zhangqh502@sina.com (Q.-H.Z.); xuqiao@vip.sina.com (Q.X.)

2 School of Materials and Energy, University of Electronic Science and Technology of China, No.4 2nd Jianshebei Road, Chengdu 610054, China; jinjuchen@uestc.edu.cn

3 College of Materials Science and Engineering, Sichuan University, No.24 1st Ring Road South, Chengdu 610041, China; jlzhu167@scu.edu.cn

* Correspondence: leixiangyang2@163.com

Received: 29 October 2019; Accepted: 21 November 2019; Published: 22 November 2019

Abstract: A high-power laser system is employed to drive the fusion ignition to realize sustainable supply of green energy according to the inertial confinement fusion theory, in which frequency-converting crystals are sealed in the terminal vacuum chamber and utilized to turn the incident laser (1053 nm) to the desired one (351 nm). However, the reflected 351 nm laser from the pellet hohlraum that goes back through the frequency-converting crystal is found to be harmful for the upstream elements that are located before the terminal chamber. In this study, a specialized coating system for the frequency-converting crystals was designed and fabricated to both ensure high output power for the fusion and reduce the reflected 351 nm laser energy by absorption. Furthermore, the structural, mechanical, and laser-damage resistant properties of this coating were investigated as well.

Keywords: high-power laser system; frequency-converting crystal coating; reflected 351 nm laser

1. Introduction

Potassium dihydrogen phosphate (KDP) and potassium dideuterium phosphate (DKDP) crystals are the very important nonlinear optical materials for the laser-driven inertial confinement fusion (ICF) [1–6]. In the high-power laser driving system, one KDP and one DKDP are combined together as a frequency-converting pair (named as FCP). It is sealed in the terminal vacuum chamber and utilized to turn the incident near-infrared laser (1053 nm, named as 1ω) to the short-wavelength one (351 nm, named as 3ω). KDP is called second harmonic generating (SHG) element to double the frequency of original laser (partially), and DKDP is called third harmonic generating (THG) element to triple the frequency of original laser as shown in Figure 1a. The incident side of SHG element suffers the irradiation of original 1ω laser, and its exit side suffers the irradiation of the residual 1ω laser and frequency-doubled laser (527 nm, named as 2ω). Meanwhile, the incident side of the THG element suffers the same irradiation as the exit side of the SHG element, and its exit side suffers the irradiation of converted 3ω laser. In order to provide enough power to drive the ignition of ICF, the output laser energy from FCP is very high [7], requiring the minimized reflecting loss for all sides. Thus, special coating system should be applied to FCP to improve its transmission and laser-induced

damage threshold (LIDT) at specific wavelengths (also shown in Figure 1a) [8]. On the other hand, inevitable reflection of 3ω laser (from the pellet hohlraum) has been proven harmful for the optical elements located before the terminal chamber by inducing irreversible laser damage [4,9–11]. Therefore, minimization of the reflected 3ω laser back through the terminal chamber should be taken into account. Unfortunately, the structure of the high-power laser system is fixed, and no room is available for an extra 3ω laser absorber, neither for the National Ignition Facility (NIF) nor Laser Megajoule (LMJ). It is assumed that applying absorption of 3ω laser at the two sides of SHG element and the incident side of THG element is a potential solution, since the 3ω laser only generates when the laser beam has passed through the THG element. The optimized coating systems based on this design are depicted in Figure 1b, which could endow the FCP element with outstanding 3ω laser output power as well as the protection of upstream elements from damaging by the reflected 3ω laser. However, literature referring to this application is rare, and related studies were hardly found. Reports from neither NIF nor LMJ have any specific statement about this application. The main spectral requirement for SHG and THG sol-gel anti-reflective coatings in LMJ is the reflectance per side ($R_{1\omega} < 0.5\%$, $R_{2\omega} < 0.5\%$, $R_{3\omega} < 0.7\%$), without the consideration to minimize the reflected 3ω laser [12]. Therefore, the exploration of such coating systems is performed in this work, and the structural, mechanical, and optical properties of this coating system have been investigated as well.

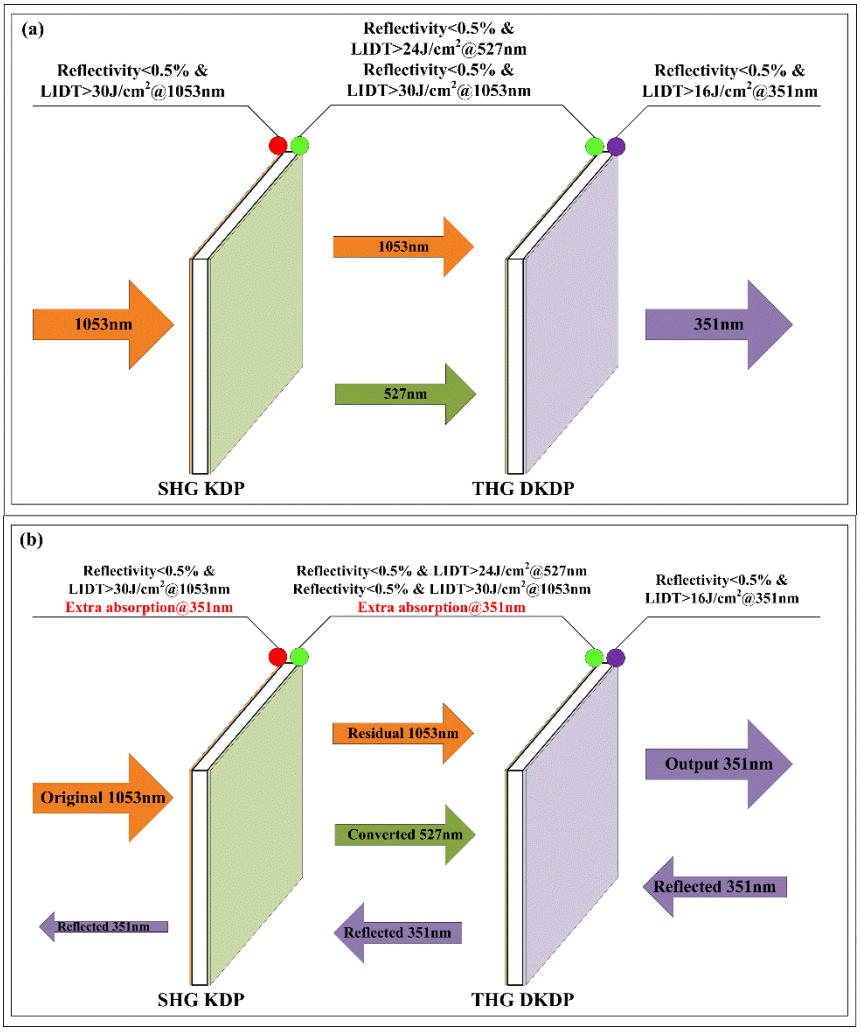

Figure 1. Schematic diagram of the frequency-converting pair (FCP) in one laser beam from high-power laser system, (**a**) original design; (**b**) optimized design.

2. Materials and Methods

2.1. Materials

Tetraethylorthosilicate (TEOS) was purchased from Sinopharm Chemical Reagent Co., Ltd. (Beijing, China). Methacryloxypropyltrimethoxysilane (MPS), tripropyleneglycoldiacrylate (TPGDA), Darocur 1173 (named as HMPP), and butanol were purchased from Shanghai Aladdin Bio-Chem Technology Co., Ltd. (Shanghai, China). Anhydrous ethanol, decane, hydrochloric acid, and ammonia water were purchased from Chengdu Kelong Chemical Co., Ltd. (Chengdu, China). The water was deionized. TEOS and MPS were distillation purified. Other chemicals were used as-purchased.

2.2. Synthesis of UV-Curable Prepolymer Sol

MPS was utilized as the matrix to perform hydrolysis and polycondensation under the addition of 1 mol equiv. acid water (HCl 0.1 M), corresponding to the stoichiometric proportion. Produced methanol was then evaporated, and fresh butanol was added after 4 h of stirring (500 rpm), adjusting the viscosity and concentration of matrix. Decane (1:3 of butanol in volume) in combination with TPGDA (1:10 of butanol in volume) was introduced to modulate the volatility of this sol and provide excess C = C group, respectively. The resulting sol was stirred for another 2 h (500 rpm) and filtered through 0.2 μm polyvinylidenefluoride (PVDF) membranes. HMPP photoinitiator (PI) with certain proportion was added and stirred before coating preparation.

2.3. Synthesis of Colloidal Porous Silica Nanoparticle Sol

The colloidal silica nanoparticle sol was prepared via the polycondensation and self-assembly of hydrolyzed TEOS, in which anhydrous ethanol and ammonium hydroxide aqueous solution (containing 30% ammonia) was applied and stirred at 6 °C for 3 h (500 rpm). The aging process was then carried out by keeping the resulting sol in a sealed glass container for three to five days at room temperature. Such sol was further refluxed for 10 h to remove the excess ammonia. The prepared colloidal suspension contained about 3.3% silica nanoparticles by weight in ethanol and was filtered through a 0.2 μm PVDF membrane filter prior to use.

2.4. Coating Preparation

Generally, three different types of coating system were needed according to the demand of FCP as shown in Figure 1a. Theoretically, a single-layer coating is needed for the incident side of SHG and exit side of THG to enhance the transmission at 1ω and both 3ω, respectively. Meanwhile, a dual-layer coating system is required for the exit side of SHG and incident side of THG to enhance the transmission at 1ω and 2ω (named as dual-wavelength coating system) simultaneously. The dual-layer coating system was fabricated by one layer with high refractive index (HRI) and another layer with low refractive index (LRI) to meet the specific spectral demand. In this study, prepolymer sols with PI concentration of 1%, 2%, and 3% by weight were prepared to fabricate the HRI layer, followed by an addition of colloidal silica nanoparticles to adjust its refractive index to proper value. A 180-s UV irradiation from a Hg lamp whose intensity was measured (EIT UVICURE Plus II) to be 200 mW/cm^2 was then applied to cure the HRI coating. This layer is the key part of this design and is discussed particularly in this work. Colloidal silica nanoparticle sol was then spin-coated under the certain velocity and time to fabricate the LRI layer over the HRI layer to form a dual-layer coating system for all sides except the exit side of THG. This special design could not only maintain the original spectral demand from high-power laser system but also induce 3ω absorption at the sides without 3ω transmission requirement. All layers were deposited under the instructions of theoretical design by TFCalc® (v.3.5) (Harvest Lane, Portland) [13–15], in order to satisfy the requirement shown in Figure 1b.

2.5. Sample Characterization

The PI behavior inside the HRI coating was analyzed using nitrogen adsorption–desorption measurement (Micromeritics ASAP 2460). Pull-off adhesion tester (Elcometer F106) was utilized to estimate the coating/substrate adhesion. Hardness of the HRI coating was extensively studied via nanoindenter (HYSTRON TI 950). Dynamic profiler (4D NanoCam Sq) was employed to characterize the surface roughness (R_q) and power spectral density (PSD) of the HRI coating. 1ω (beam diameter is about 610 μm, repetition frequency is 1 Hz, measurement error is within 6%) and 2ω (beam diameter is about 540 μm, repetition frequency is 1 Hz, measurement error is within 9%) LIDT of the HRI coating was determined using R-on-1 mode (laser was focused on one spot, and its energy was continuously increased with each pulse until the coating was broken), in which 100 sampling spots were tested in each sample. For the dual-layer systems, transmission spectra were recorded using UV-Vis-NIR spectrometer (PE Lambda 950) in the range of 300 nm to 1100 nm.

3. Results and Discussion

Based on the design from TFClac®, the transmission at 1ω can achieve nearly 100%; however, the transmission at 3ω is as high as 98.4% for mono-layer 1ω coating. As for dual-wavelength coating system, the transmission could exceed 99.5% at both 1ω and 2ω, while the transmission at 3ω was about 96%. However, the transmission at 3ω still needs further reduction because about 2–10% of the original 3ω laser energy could be reflected according to different hohlraum structures [16,17], and this energy is yet quite harmful. Since UV curing has been applied for the coatings in high-power laser system [18], the UV PI is considered not only to be able to cure the HRI coating but also to absorb the reflected 3ω laser energy. In this study, optimized coating design using TFCalc® software and 3ω energy absorption using UV PI are applied for the FCP in order to meet the spectral demand shown in Figure 1b.

Optimized coating design for 1ω coating system and dual-wavelength coating system was first performed and the results are listed in Table 1. In order to insert the HRI coating into 1ω coating system to endow it with 3ω absorption, the transmission of 1ω coating at 1ω has been sacrificed a little. Therefore, it is found that these two coating systems have nearly the same optimal parameters. The transmission at 1ω and 2ω could both reach 99.6% while that at 3ω was about 95.7% (see Table 1). Thus, 1ω coating system and dual-wavelength coating system can be consolidated as one coating system. The preparation of this consolidated coating system was divided into two steps, one was to deposit HRI layers with refractive index around 1.38 and thickness about 127 nm using prepolymer sols, the other was to utilize the colloidal silica nanoparticle sol to prepare LRI layer with refractive index around 1.22 and thickness about 144 nm over the cured HRI layer.

Table 1. Optimized coating design for 1ω coating system and dual-wavelength coating system from TFCalc®.

Type	HRI Layer		LRI Layer		Transmission (%)		
	n	d (nm)	n	d (nm)	351 nm	527 nm	1053 nm
1ω coating system	1.38	127.16	1.22	144.31	95.7	99.6	99.6
Dual-wavelength coating system	1.38	127.18	1.22	144.29	95.7	99.6	99.6

A series of consolidated coating systems was fabricated by applying different PI concentration (1%, 2%, and 3%) to form the HRI layer. Nitrogen adsorption–desorption analysis was performed to figure out the behavior of PI molecule inside the HRI coatings. Specific surface area of the coating was analyzed by Brunauer–Emmett–Teller (BET) method, and pore size distribution was analyzed using Barrett–Joyner–Halenda (BJH) method [19–24]. It is found from Figure 2 that contributing pore size for the pore volume is below 10 nm, implying that large pores hardly existed inside the coating. In addition, the inset of Figure 2 shows that bigger pores contribute more for the pore volume with the

increase of PI concentration, indicating that the PI molecule started the occupancy from the smaller pores inside the coating. Moreover, the specific surface area of the coating gradually decreases with the increase of PI addition (listed in the upper right of Figure 2), which confirms the occupancy of micropores by the increasing PI molecule. The coating refractive index increases with the increasing of PI concentration because of the decrease of coating porosity. Thus, further addition of porous silica nanoparticles is applied to keep the refractive index of HRI coating at 1.38 under different PI doping amounts.

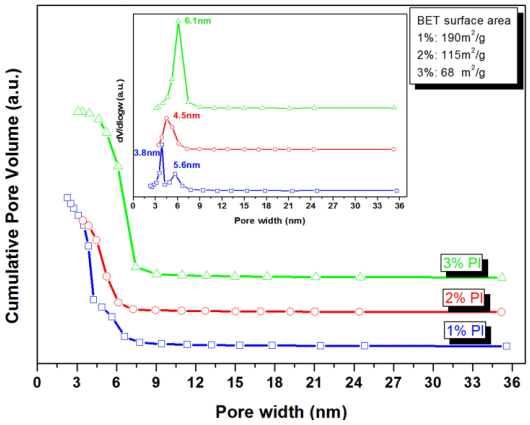

Figure 2. N_2 adsorption–desorption results of HRI coatings with different photoinitiator (PI) concentrations.

Mechanical properties are very crucial for the practical application of high-power laser coatings. Coating/substrate adhesion determines the lifetime and hardness decides the reliability of the coating. Figure 3 illustrates the adhesion and hardness of the HRI coating with different PI concentrations. Each sample was tested at three different places, and the results displayed in Figure 3 are the average value. Coating/substrate adhesion of three samples almost stays the same around 1.7 MPa, indicating no obvious effect of PI molecule on the adhesion. Meanwhile, coating hardness exhibits prominent variation along with the increasing of PI concentration. An increase followed by a decrease is observed in the coating hardness results, which may be ascribed to the role switch of the PI molecule. Increasing PI at the beginning provides more free radicals that help to facilitate the curing of prepolymer, but further increasing of PI concentration might separate the prepolymer and prevent it from cross-linking, which means the PI molecule actually acts partly as photoinitiator and partly as isolator. It acts more like isolator than photoinitiator and incomplete curing of coating takes place if its concentration increases.

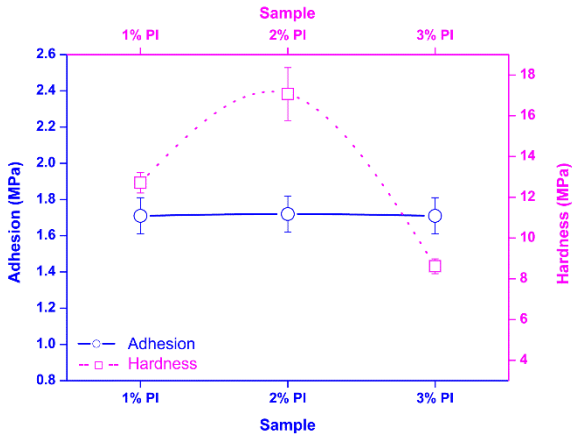

Figure 3. Adhesion and hardness of high refractive index (HRI) coatings with different PI concentrations.

LIDT is the acknowledged standard to estimate the laser-damage resistance, which is an important characteristic for the coatings being applied in the high-power laser system, and such a test has been performed on the HRI coatings with different PI concentrations. As the HRI coating only suffers 1ω and 2ω laser, its 1ω and 2ω LIDT has been verified using R-on-1 mode. Figure 4 depicts the testing results of different HRI coatings, in which the LIDT of 1ω is estimated to be around 48 J/cm^2 (5 ns equiv.) and that of 2ω is about 32 J/cm^2 (5 ns equiv.). No obvious variation trend can be observed for the LIDT with the increasing of PI concentration, indicating that the addition of UV PI does not deteriorate the 1ω and 2ω laser-damage resistance of coating.

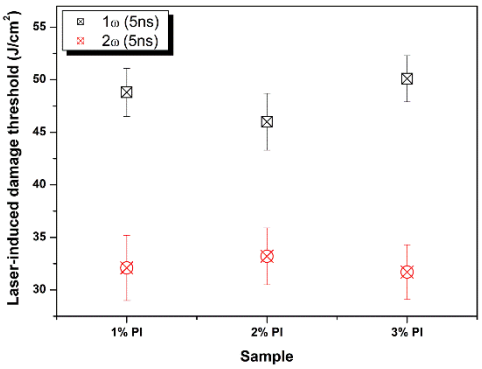

Figure 4. 1ω and 2ω laser-induced damage threshold (LIDT) of HRI coatings with different PI concentrations.

In the high-power laser system, some other key characteristics that influence the transmission quality of the laser beam also need to be taken into account, especially for the roughness, such as the R_q (high-frequency spatial part) and PSD (middle-frequency spatial part) [25–27]. The R_q (0.01–0.12 mm) results of HRI coating are illustrated in Figure 5a, in which a gradual but slight increase can be observed while the PI concentration increases. Figure 5b shows the PSD2 (0.12–2.5 mm) results of HRI coating with different PI concentrations. Nearly the same trend as the R_q results is noticed, but the variation is a little larger than that of R_q. This means that the addition of the PI molecule gradually degrades the R_q and PSD2 of HRI coating and deteriorates the transmission quality of high-power laser beam further. This is assumed to be attributed to the behavior of the PI molecule mentioned above. With the increasing of the PI molecule, more and more micropores are occupied inside the coating, resulting in coating structure deformation (as demonstrated in Figure 6) and unexpected degradation of R_q and PSD2.

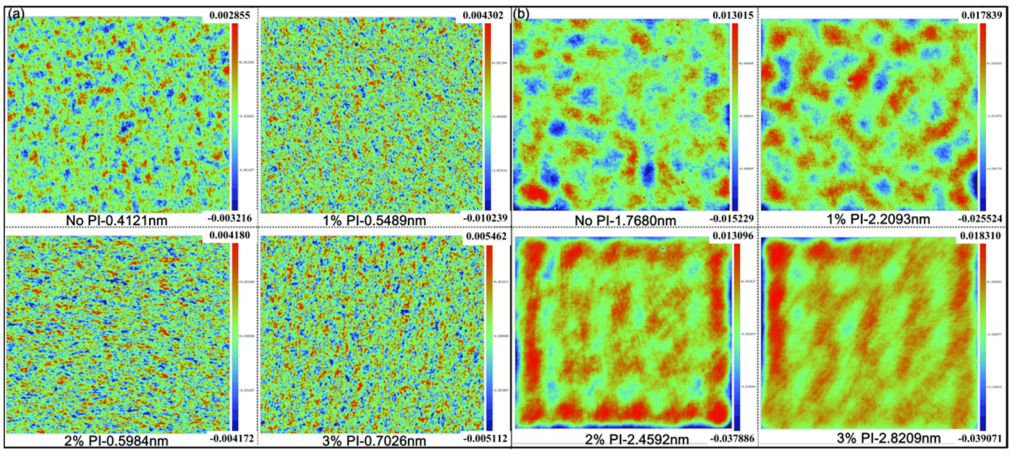

Figure 5. (**a**) Surface roughness and (**b**) power spectral density (PSD)2 of HRI coatings with different PI concentrations.

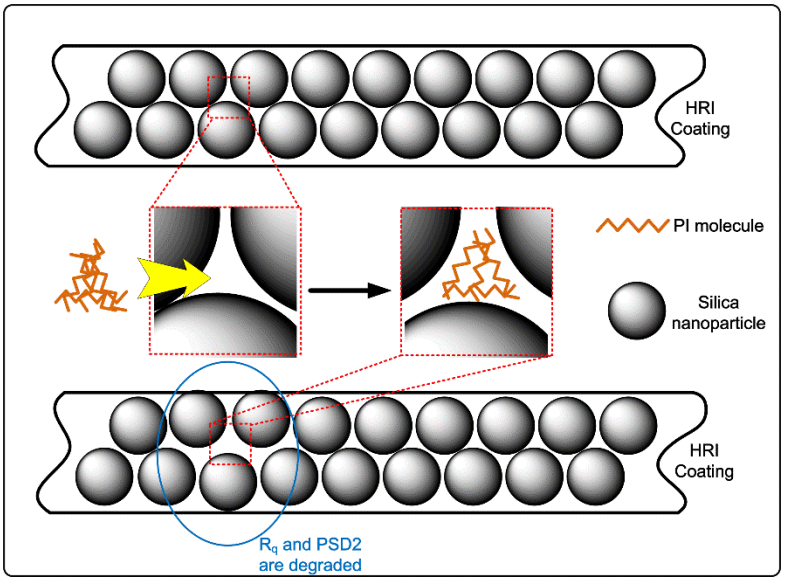

Figure 6. Schematic diagram of HRI coating deformation due to PI addition.

Figure 7 demonstrates the transmission spectra of the consolidated coating system with different PI concentrations in HRI coating. It is found that the transmission at 3ω keeps decreasing with the increasing of PI concentration and drops below 90% when PI concentration reaches 3%, proving the predicted absorption of 3ω laser energy by UV PI. It is also found that the transmission at 1ω hardly changes, but the transmission at 2ω slightly decreases after the addition of PI, which might be ascribed to the refractive index variation caused by the PI occupancy of micropores inside the coating (the transmission at 2ω is more sensitive to the refractive index than that at 1ω because 2ω is located around a peak in the spectrum). This drawback can be overcome by the precise control of coating refractive index, and related study is currently in progress. Unfortunately, the sol becomes invalid for neither coating nor curing if PI concentration keeps increasing over 4% because the presence of too much PI molecule affects the original status of sol (like viscosity, volatilization rate, matrix concentration) and prevents the MPS prepolymer from cross-linking (leading to incomplete curing of the coating).

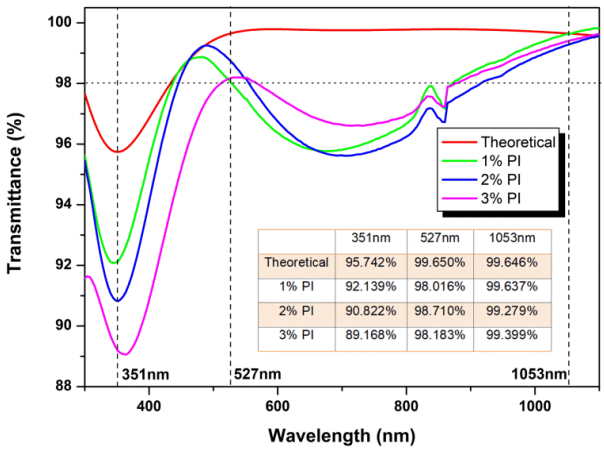

	351nm	527nm	1053nm
Theoretical	95.742%	99.650%	99.646%
1% PI	92.139%	98.016%	99.637%
2% PI	90.822%	98.710%	99.279%
3% PI	89.168%	98.183%	99.399%

Figure 7. Transmission spectra of the dual-layer consolidated coating system with (different PI concentrations) and without PI (theoretical simulation).

4. Conclusions

UV-cured silicone high-refractive-index coatings with different photoinitiator concentrations were fabricated. The addition of excess photoinitiator can provide extra absorption at 351 nm while

maintaining high transmission at 1053 nm and 527 nm for the coating. The laser-damage resistance of such coating was above 45 J/cm^2 at 1053 nm (5 ns equiv.) and 30 J/cm^2 at 527 nm (5 ns equiv.). The adhesion of the coating was proven to be almost free for the photoinitiator addition, but the hardness, R_q, and PSD2 of the coating degraded if the PI concentration increased. Transmission spectra of the optimized dual-layer coating system proved the predicted absorption of 351 nm energy, while the refractive index of the HRI coating should be precisely controlled if high transmission at both 1053 nm and 527 nm is desired. This provides a potential solution to both ensure the high output power of the 351 nm laser and protect the upstream optical elements from damage by reflected 351 nm laser in the high-power laser system.

Author Contributions: X.-R.D. was responsible for the writing of original draft. W.Y. was the main operator of the investigation experiments. H.-H.H. performed the simulation and optimization of coating systems by TFCalc® software. Q.-H.Z. provided and arranged the related resources for this work. Q.X. was the supervisor of this work. J.-J.C. and J.-L.Z. carried out the formal analysis of this work. X.-Y.L. was in charge of the review and editing of this paper.

Funding: This work was supported by the Opening Project of Shanghai Key Laboratory of Special Artificial Microstructure Materials and Technology (grant No. Ammt2019A-4).

Acknowledgments: Special thanks to Jun Shen and Xiaodong Wang for funding acquisition.

Conflicts of Interest: The authors declare that there is no conflict of interest in this work.

References

1. Eimerl, D.; Auerbach, J.M.; Milonni, P.W. Paraxial wave theory of second and third harmonic generation in uniaxial crystals. *J. Mod. Opt.* **1995**, *42*, 1037–1067. [CrossRef]
2. Miller, G.H.; Moses, E.I.; Wuest, C.R. The national ignition facility. *Opt. Eng.* **2004**, *43*, 2841–2853. [CrossRef]
3. Zhang, Q.H.; Deng, X.R.; Yang, W.; Hui, H.H.; Wei, Y.W.; Chen, J.J. Comparative study on cracking behavior of sol-gel silica antireflective coating for high-powered laser system. *Eng. Fail. Anal.* **2017**, *82*, 64–71. [CrossRef]
4. Moses, E.I.; Wuest, C.R. The national ignition facility: Laser performance and first experiments. *Fusion Sci. Technol.* **2005**, *47*, 314–322. [CrossRef]
5. Haynam, C.A.; Wegner, P.J.; Auerbach, J.M.; Bowers, M.W.; Dixit, S.N.; Erbert, G.V.; Heestand, G.M.; Henesian, M.A.; Hermann, M.R.; Jancaitis, K.S.; et al. National ignition facility laser performance status. *Appl. Opt.* **2007**, *46*, 3276–3303. [CrossRef]
6. Yang, W.; Lei, X.Y.; Hui, H.H.; Zhang, Q.H.; Deng, X.R. Fabrication of refractive index tunable coating with moisture-resistant function for high-power laser systems based on homogeneous embedding of surface-modified nanoparticles. *Molecules* **2018**, *23*, 1105. [CrossRef]
7. Meyer-ter-Vehn, J. Prospects of inertial confinement fusion. *Plasma Phys. Contr. Fusion* **1997**, *39*, B39–B45. [CrossRef]
8. Zhang, Q.; Wei, Y.; Yang, W.; Hui, H.; Deng, X.; Wang, J.; Xu, Q.; Shen, J. Improvement on contamination resistance to volatile organics and moisture of sol-gel silica antireflective coating for 351 nm laser system by structural modulation with fluorinated compounds. *RSC Adv.* **2015**, *5*, 4529–4536. [CrossRef]
9. Liu, H.; Jensen, L.; Ma, P.; Ristau, D. Stress compensated anti-reflection coating for high power laser deposited with IBS SiO_2 and ALD Al_2O_3. *Appl. Surf. Sci.* **2019**, *476*, 521–527. [CrossRef]
10. Dereure, C.; Hall, R.; Baber, F.; Loison, D.; Lescoute, E.; Guin, J.P.; Sangleboeuf, J.C.; Berthe, L.; Nivard, M.; Guven, I. Laser induced dynamic fracture of fused silica: Experiments and simulations. *J. Non-Cryst. Solids* **2019**, *511*, 125–139. [CrossRef]
11. Xu, J.M.; Chen, M.M.; Liu, Z.Q.; Wang, J.; Liu, L.M.; Han, Z.C.; Xu, H.B. Investigation of wavelength effects on polycrystalline silicon damages using nanosecond pulse laser irradiation. *J. Mater. Process Technol.* **2019**, *267*, 159–166. [CrossRef]
12. Lavastre, E.A.; Raze, G.; Gaborit, G.; Mainguy, S.; Pellegrini, C.; Cavaro, S.; Lebeaux, I. Metrologies of LMJ sol-gel anti-reflective coatings in the production line. In *Optical Interference Coatings*; Tilsch, M., Ristau, D., Eds.; Optical Society of America: Washington, DC, USA, 2013; p. ThD.2.

13. Hu, D.; Liu, D.; Zhang, J.; Wu, L.; Li, W. Preparation and stability study of broadband anti-reflection coatings and application research for CdTe solar cell. *Opt. Mater.* **2018**, *77*, 132–139. [CrossRef]
14. Khan, S.B.; Irfan, S.; Zheng, Z.; Lee, S.L. Influence of refractive index on antireflectance efficiency of thin films. *Materials* **2019**, *12*, 1483. [CrossRef] [PubMed]
15. Ye, L.; Ge, X.; Wang, X.; Hui, Z.; Zhang, Y. Design and preparation of durable double-layer non-quarter-wave antireflective coatings. *Ceram. Int.* **2019**, *45*, 8504–8509. [CrossRef]
16. Di Nicola, J.M.; Bond, T.; Bowers, M.; Chang, L.; Hermann, M.; House, R.; Lewis, T.; Manes, K.; Mennerat, G.; MacGowan, B. The national ignition facility: Laser performance status and performance quad results at elevated energy. *Nucl. Fusion* **2019**, *59*, 032004. [CrossRef]
17. Meezan, N.B.; Edwards, M.J.; Hurricane, O.A.; Patel, P.K.; Callahan, D.A.; Hsing, W.W.; Town, R.P.J.; Albert, F.; Amendt, P.A.; Berzak Hopkins, L.F.; et al. Indirect drive ignition at the national ignition facility. *Plasma Phys. Contr. Fusion* **2017**, *59*, 014021. [CrossRef]
18. Deng, X.R.; Yang, W.; Zhang, Q.H.; Hui, H.H.; Wei, Y.W.; Wang, J.; Xu, Q.; Lei, X.Y.; Chen, J.J.; Zhu, J.L. Fabrication of UV-curable silicone coating with high transmittance and laser-induced damage threshold for high-power laser system. *J. Sol-Gel Sci. Technol.* **2018**, *88*, 249–254. [CrossRef]
19. Garcia-Briones, G.S.; Ocampo-Perez, R.; Gomez-Duran, C.F.A.; Neri-Gomez, T.; Palestino, G. Porous silicon microcarriers for extended release of metformin: Design, biological evaluation and 3D kinetics modeling. *Chem. Eng. J.* **2019**, *365*, 415–428. [CrossRef]
20. Radi, S.; Abiad, C.E.; Moura, N.M.M.; Faustino, M.A.F.; Neves, M.G.P.M.S. New hybrid adsorbent based on porphyrin functionalized silica for heavy metals removal: Synthesis, characterization, isotherms, kinetics and thermodynamics studies. *J. Hazard. Mater.* **2019**, *370*, 80–90. [CrossRef]
21. Liu, Y.; Yang, W.; He, X.; Hou, H. Tailored synthesis of amorphous SiCNO mesoporous fibers through combining a facile electrospinning process and microwave-assisted pyrolysis. *Ceram. Int.* **2019**, *45*, 8640–8645. [CrossRef]
22. Prete, M.C.; Teixeira Tarley, C.R. Bisphenol A adsorption in aqueous medium by investigating organic and inorganic components of hybrid polymer (polyvinylpyridine/SiO_2/APTMS). *Chem. Eng. J.* **2019**, *367*, 102–114. [CrossRef]
23. Bhavsar, D.; Gajjar, J.; Sawant, K. Formulation and development of smart pH responsive mesoporous silica nanoparticles for breast cancer targeted delivery of anastrozole: In vitro and in vivo characterizations. *Micropor. Mesopor. Mater.* **2019**, *279*, 107–116. [CrossRef]
24. Ma, S.; Zhang, L.; Wang, S.; Zhang, H.; You, X.; Ou, J.; Ye, M.; Wei, Y. Preparation of epoxy-functionalized hierarchically porous hybrid monoliths via free radical polymerization and application in HILIC enrichment of glycopeptides. *Anal. Chim. Acta* **2019**, *1058*, 97–106. [CrossRef] [PubMed]
25. Huang, W.Q.; Zhang, Y.; Wang, W.Y.; Geng, Y.C.; Liu, L.Q. Research on power spectral density after nonlinear propagation in high-power solid state laser. *Proc. SPIE* **2015**, *9255*, 92551F.
26. Aikens, D.M.; Roussel, A.; Bray, M. Derivation of preliminary specifications for transmitted wavefront and surface roughness for large optics used in inertial confinement fusion. *Proc. SPIE* **1995**, *2633*, 350–360.
27. Wolfe, C.R.; Lawson, J.K. Measurement and analysis of wavefront structure from large-aperture ICF optics. *Proc. SPIE* **1995**, *2633*, 361–385.